K_{2P} channel TWK-40 Regulates a Rhythmic Behavior in *C. elegans*

Zhongpu Yue [1,2#], Yongning Zhang [2#], Bin Yu [2#], Yueqing Xu [3#], Lili Chen [2], Yi Li [2], Jyothsna Chitturi [4], Jun Meng [4], Wesley Hung [4], Sonia El Mouridi [5,6], Thomas Boulin [5], Cuntai Zhang [1], Mei Zhen [4], Shangbang Gao [1,2]*

1. Department of Geriatrics, Tongji Hospital of Tongji Medical College, Huazhong University of Science and Technology, Wuhan, China

2. Key Laboratory of Molecular Biophysics of the Ministry of Education, College of Life Science and Technology, Huazhong University of Science and Technology, Wuhan 430074, China

3. College of Biomedical Engineering, South-Central University for Nationalities, Wuhan 430074, China.

4. Lunenfeld-Tanenbaum Research Institute, Mount Sinai Hospital, University of Toronto, Toronto, Ontario M5G 1X5, Canada

5. Univ Lyon, Université Claude Bernard Lyon 1, MeLiS, CNRS UMR 5284, INSERM U1314, Institut NeuroMyoGène, Lyon 69008, France

6. King Abdullah University of Science and Technology (KAUST), Biological and Environmental Sciences and Engineering Division (BESE), Thuwal 23955–6900, Kingdom of Saudi Arabia

[#] **Equal contributions**

* **Correspondence**: sgao@hust.edu.cn

Running title: TWK-40 regulates defecation rhythm

Key words: *twk-40*, motor rhythm, defecation, Ca^{2+} oscillation, K_{2P} channel, resting membrane potential

Abstract

Background potassium (K^+) currents, conducted by two-pore domain K^+ (K_{2P}) channels, are critical for the stabilization of the membrane potential. The effect of K_{2P} channels on motor rhythm remains enigmatic. We show here that the K_{2P} TWK-40 regulates the rhythmic defecation motor program (DMP) in *Caenorhabditis elegans*. Disrupting TWK-40 suppresses the expulsion defects of *nlp-40* and *aex-2* mutants. By contrast, a gain-of-function (*gf*) mutant of *twk-40* significantly reduces the expulsion frequency per DMP cycle. *In situ* whole-cell patch clamping demonstrates that TWK-40 forms an outward current that hyperpolarize the resting membrane potential of DVB neuron. In addition, TWK-40 substantially contributes to the rhythmic activity of DVB. Specifically, DVB Ca^{2+} oscillations exhibit obvious defects in *twk-40* mutants. Expression of TWK-40(*gf*) in DVB recapitulates the expulsion deficiency of the *twk-40(gf)* mutant, and inhibits DVB Ca^{2+} oscillations in both wild-type and *twk-40(lf)* animals. Moreover, DVB innervated enteric muscles also exhibit rhythmic Ca^{2+} defects. Taken together, these results demonstrate that TWK-40 is an essential inhibitor of DMP, thus revealing a cellular mechanism linking K_{2P} channels with rhythmic motor activity.

42 **Introduction**

43 Two-pore domain potassium (K_{2P}) channels conduct K^+ leak currents. In contrast to
44 voltage-gated K^+ channels, K_{2P}s are mostly voltage-independent and non-inactivating
45 channels, which stabilize the cell's resting membrane potential (Enyedi and Czirjak,
46 2010). Along with most K_{2P} channels profiling by heterologous expression systems or in
47 cultured primary cells, the channel associated behaviors and the intrinsic physiological
48 characterization of specific K_{2P} channel have remained largely unknown.

49 The human genome encodes 15 K_{2P} channels, which are grouped into six families
50 based on their functional resemblance and structural similarity (Goldstein et al., 2005;
51 Lesage and Lazdunski, 2000). Aberrant functions of K_{2P} channels have been implicated
52 in various disorders associated with genetic variation. For example, mutations of human
53 TASK-3 (KCNK9 p.Gly236Arg) cause *KCNK9* Imprinting Syndrome, a pediatric
54 neurodevelopmental disease with severe feeding difficulties, delayed development and
55 intellectual disability (Graham et al., 2016). With predicted conservation of amino acid
56 sequences across species, K_{2P} channels associated genetic and functional investigations in
57 animal models are emerging (Buckingham et al., 2005). For instance, cardiac-specific
58 inactivation or overexpression of Ork1, a *Drosophila* two-pore domain potassium
59 channel, led to an increase or a complete arrest of fly heart beating, respectively (Lalevee
60 et al., 2006).

61 The nematode *Caenorhabditis elegans* (or *C. elegans*) genome contains a large family
62 with at least 47 K_{2P} genes (Bargmann, 1998; Buckingham et al., 2005). This large set of
63 K_{2P} channels may allow for exceptionally fine 'tuning' of the firing activity of individual
64 cells within the very compact (300 neurons) nematode nervous system (Witvliet et al.,

65 2021; Salkoff et al., 2001). Encouraged by the increasing understanding of the molecular
66 and cellular wiring of the worm's neural network (White et al., 1986; Bargmann, 1998;
67 Cook et al., 2019; Witvliet et al., 2021; Taylor et al. 2021), we use *C. elegans* to explore
68 the functional complexity of K_{2P} channels as potential regulators of rhythmic behaviors *in*
69 *vivo* (Ben Soussia et al., 2019; Wang et al., 1999).

70 The *C. elegans* defecation motor program (DMP) exhibits a highly coordinated
71 short-term rhythm. It is achieved by periodically activating a stereotyped sequence of
72 muscle contractions, including the initial contraction of posterior body wall muscles
73 (pBoc), followed by the second contraction of anterior body wall muscles (aBoc), and the
74 final contraction of enteric muscles (EMC) (Thomas, 1990). Driven by the synchronizing
75 activity of electrically-coupled DVB and AVL motor neurons (Choi et al., 2021), EMC
76 leads to the robust expulsion (Exp) of gut contents (**Figure 1A**) (Dal Santo et al., 1999;
77 Liu and Thomas, 1994). Unlike most rhythmic motor circuits that are composed of a
78 central pattern generator (CPG) neural network or self-oscillating pacemaker neurons
79 (Marder and Calabrese, 1996), the expulsion rhythm is precisely timed by endogenous
80 calcium oscillation signals from the intestine (Branicky and Hekimi, 2006; McIntire et
81 al., 1993a). The intestinal IP_3 receptor/*itr-1*-driven pacemaker Ca^{2+} oscillations trigger a
82 Ca^{2+}-dependent secretion of neuropeptide NLP-40, which activates the neuronal G
83 protein-coupled receptor (GPCR) AEX-2 in DVB and AVL (Mahoney et al., 2008;
84 Nehrke et al., 2008; Teramoto and Iwasaki, 2006; Wang et al., 2013). GABA release
85 from DVB (McIntire et al., 1993b), cyclically initiated by NLP-40 (Wang et al., 2013),
86 activates the muscular excitatory GABA-gated cation channel EXP-1 to drive the final
87 contraction of enteric muscles (**Figure 1B**) (Beg and Jorgensen, 2003). Deficiency of

88 either NLP-40, AEX-2 or EXP-1 results in serious expulsion defects in *C. elegans*. Thus,
89 the intestinal Ca^{2+} oscillation sets the instructive timing signal of the expulsion rhythm
90 (Branicky and Hekimi, 2006; McIntire et al., 1993a). However, the cellular processes that
91 control the expulsion rhythm in the intestine-neuron-muscle circuit are still unclear.
92 We show here that loss of function of *twk-40* – a two-pore domain potassium
93 channel subunit – specifically suppresses the expulsion defects of *nlp-40* and *aex-2*
94 mutants, but not of *exp-1* mutant. TWK-40 exhibits the common structural features of
95 K_{2P} channel based on sequence analyses. The single subunit of TWK-40 has four
96 transmembrane regions and two pore-forming domains (**Figure 2A**), which exhibit
97 sequence similarity with the mammalian TASK (tandem-pore-acid-sensing K^+) subfamily
98 (**Supplementary Figure 1A**). A gain of function mutant of *twk-40(bln336)*, generated by
99 CRISPR/Cas9 gene editing (Ben Soussia et al., 2019), induces an expulsion defect by
100 reducing the frequency of expulsion per DMP cycle. Moreover, *in-situ* whole-cell patch
101 clamping revealed a *twk-40*-dependent outward K^+ current that regulates the resting
102 membrane potential in DVB neurons, in which the resting membrane potential (RMP)
103 was depolarized in *twk-40(lf)* and hyperpolarized in *twk-40(gf)* mutant, respectively. In
104 combination with real-time Ca^{2+} imaging, we provide several lines of evidence that
105 demonstrate that TWK-40 regulates rhythmic motor behaviors – including defecation –
106 by cell-autonomously regulating DVB's resting membrane potential.
107 Remarkably, we also found recently that TWK-40 modulates global locomotor
108 activity by regulating the activity of the AVA premotor interneuron (Meng et al., 2022).
109 Briefly, *twk-40(lf)* mutant animals exhibit exaggerated body bends during both forward
110 and backward movement, and more frequent and prolonged reversals. *twk-40(gf)* mutant

111 animals, by contrast, exhibit strongly altered locomotion including obvious decreased
112 body bending and velocity in both rhythmic forward and backward undulation.
113 Heterologous expression of the TWK-40 in HEK293 cells produced a voltage-insensitive
114 K^+ selective K_{2P}-like ion channel. Therefore, the K_{2P} channel TWK-40 is required for the
115 generation of multiple motor rhythms, including the defecation and locomotion motor
116 programs.

117 **Results**

118 ***twk-40(lf) suppresses the expulsion defect of nlp-40 and aex-2 mutants***

119 To determine a potential role of the TWK-40 K_{2P} channel in the cellular mechanisms
120 controlling rhythmic DMP activity, we took advantage of three *exp* mutants that disrupt
121 DMP in different tissues within the expulsion motor circuit (**Figure 1B**). First, *nlp-*
122 *40(tm4085)*, an instructive neuropeptide from the intestinal pacemaker that delivers
123 temporal information to the DVB neuron (Wang et al., 2013). Second, *aex-2(sa3)*, a G-
124 protein-coupled receptor that functions as the DVB receptor for NLP-40 (Mahoney et al.,
125 2008; Wang et al., 2013). And the third, *exp-1(sa6)*, which encodes an excitatory GABA
126 receptor expressed in enteric muscles (Beg and Jorgensen, 2003; Lee et al., 2005). Loss-
127 of-function mutants of these genes induced severe expulsion defects (**Figure 1C, E, G**)
128 by disrupting the normal function of the intestine, DVB neuron and enteric muscles,
129 respectively.

130 We reasoned that a loss of the potassium conductance *twk-40* would increase the
131 excitability of cells within the circuit and compensate the inhibitory effect of the *nlp-40*,
132 *aex-2*, or *exp-1* mutations. Hence, we combined the *twk-40* allele *hp834* (Figure 2A)
133 (Meng et al., 2022) with each DMP mutation. *hp834* contains a 7 bp deletion of the

134 sequence (GTTCGAG) at the base of 127-133 exon before the first pore-forming domain
135 of T28A8.1a (Figure 2A), causing a frameshift and subsequent premature stop codon of
136 *twk-40a* (Meng et al., 2022), one of three annotated isoforms of *twk-40*
137 (www.wormbase.org). We found that *twk-40(hp834)* significantly improved the
138 expulsion defect in *nlp-40* and *aex-2* mutants (**Figure 1C-F**). Specifically, the expulsion
139 frequency per DMP was increased in *nlp-40(tm4085); twk-40(hp834)* or *aex-2(sa3); twk-*
140 *40(hp834)*, when compared to the single mutants of *nlp-40(tm4085)* and *aex-2(sa3)*,
141 respectively (**Figure 1C-F**). Similar expulsion defect suppression was observed in
142 another *twk-40(lf)* allele *hp733* (**Supplementary Figure 1B**), which harbors a missense
143 mutation that changes an amino acid at the end of the first transmembrane domain
144 (E58K) (Meng et al., 2022). By contrast, no substantial suppression of the expulsion
145 defect of *exp-1* mutants was observed for either loss-of-function allele of *twk-40*. Indeed,
146 no difference in expulsion frequency was observed between *exp-1(sa6)* and *exp-1(sa6);*
147 *twk-40(hp834)* or *exp-1(sa6); twk-40(hp733)* double mutants, respectively (**Figure 1G,**
148 **H, Supplementary Figure 1B**). These results demonstrated that *twk-40* is selectively
149 required for rhythmic defecation regulation, upstream of *exp-1*.

150 ***A twk-40 gain-of-function mutation reduces expulsion frequency***

151 The selective suppression of *exp* defects in distinct *exp* mutants suggested that *twk-*
152 *40, per se,* may regulate the DMP. Indeed, in *twk-40(hp834, lf)* single mutants, the
153 expulsion number was modestly but significantly increased (13.87±0.21/10 min)
154 compared to wild-type animals (12.97±0.19/10 min) (**Figure 2C, D**). Similar results were
155 also observed in *twk-40(hp733)* mutants. These results confirm that *twk-40* regulates the
156 DMP negatively.

157 To further confirm the involvement of *twk-40* in the defecation motor program, we
158 examined the expulsion step in a gain-of-function mutant allele of *twk-40, bln336*
159 (**Figure 2A**). These mutants harbor a pan-K_{2P} activating mutation (Ben Soussia et al.,
160 2019) that promotes the gating of vertebrate and invertebrate K_{2P} channels. Indeed,
161 heterologous expression of the corresponding TWK-40(L159N) channel in HEK293 cells
162 showed ~5 fold current increase from the wild-type TWK-40 (Meng et al., 2022).
163 Consistent with an inhibitory function of *twk-40*, we observed a strongly reduced
164 expulsion frequency (4.8±0.25/10 min) in *twk-40(bln336, L159N*) animals, i.e.
165 approximately 25% of wild type (12.97±0.19/10 min) (**Figure 2C, D**). Thus, gain-of-
166 function of *twk-40* inhibits the expulsion rhythm, which encouraged us to further
167 investigate the functional effects of *twk-40* loss- and gain-of-function mutants.

168 ***twk-40 regulates expulsion in the DVB neuron***

169 To pinpoint the exact role of *twk-40* in the DMP, we first assessed its cellular focus
170 of action. Loss of *twk-40* suppressed the *exp* defect of *nlp-40* and *aex-2* mutants but not
171 of *exp-1*, indicating that *twk-40* regulates the expulsion frequency from the intestine
172 and/or expulsion neurons. Indeed, functional TWK-40 driven by a small fragment of its
173 upstream region (P*twk-40*::TWK-40::sl2dGFP, Methods) revealed the expression
174 exclusively in the nervous system and intestine (**Figure 2B**). The neuronal expression
175 pattern includes the excitatory ventral motor neurons (A and B types), but no expression
176 was observed in D-motor neurons. Meanwhile, sparse labeling of head and tail neurons
177 was also observed, including the DVC interneuron (strong) and the GABAergic DVB
178 motor neuron/interneuron (moderate) (**Figure 2B**).

179 We then systematically tested the tissue or cell requirements of *twk-40* for the
180 expulsion behavior. A wild-type TWK-40 cDNA driven by different promoters was
181 expressed in *twk-40(bln336, gf)* mutant, in an attempt to reduce its severe *exp* defect.
182 Expression of wild-type TWK-40 (i.e., TWK-40(WT)) by the short promoter P*twk-40*
183 (Methods) rescued the animal's expulsion frequency to 55.5±4.5% (**Figure 2E**).
184 Expression of TWK-40(WT) in GABAergic DVB/AVL and D-motor neurons (driven by
185 a P*unc-47* promoter fragment), also significantly restored the DMP (67.7±6.4%). In
186 contrast, expression of the TWK-40(WT) in the intestine (driven by P*ges-1* promoter,
187 33.2±1.9%) (**Supplementary Figure S1C**) or D-motor neurons (driven by a short P*unc-*
188 *25* promoter, 33.8±5.6%, Methods), however, did not restore a normal expulsion
189 frequency (**Figure 2E**). Therefore, consistent with the expression pattern, these results
190 suggest that regulation of the expulsion rhythm by *twk-40* requires DVB neurons.
191 To further confirm this notion, we ectopically expressed the TWK-40(L159N) gain-
192 of-function mutant in DVB neurons. Indeed, in the wild-type N2 background, TWK-
193 40(L159N) expression in DVB (using its own promoter or P*unc-47*) resembled the
194 expulsion defect as found in *twk-40(bln336)* mutant animals, exhibiting strongly reduced
195 expulsion frequency per cycle (**Figure 2F**). TWK-40(L159N) expression only in D-MNs
196 (by the short P*unc-25* promoter), however, could not replicate this defect. Similar
197 phenotypes were also observed by expressing TWK-40(L159N) in a *twk-40(lf)* mutant
198 context (**Figure 2G**).
199 Taken together, these results demonstrate that *twk-40* is sufficient and necessary in
200 DVB neurons for the regulation of the expulsion rhythm.

201 ***Rhythmic Ca^{2+} oscillation of the DVB neuron is disrupted in twk-40 mutants***

202 To determine whether *twk-40* directly regulates DVB's neuronal activity, we
203 performed Ca^{2+} imaging in animals expressing the genetically encoded Ca^{2+} sensor
204 GCaMP6s in the DVB neuron (**Figure 3Ai**). DVB exhibited tight correlation of rhythmic
205 Ca^{2+} oscillations with cyclic expulsion behavior (Wang and Sieburth, 2013). In wild-type
206 animals, DVB fired periodic Ca^{2+} spikes (or Ca^{2+} oscillations) with a frequency of
207 4.5±0.3 Hz/300s (**Figure 3Aii**). In *twk-40(bln336, gf)* mutants, the frequency of Ca^{2+}
208 spikes was significantly reduced to 3.2±0.3 Hz/300s (**Figure 3B, C**). Interestingly, the
209 Ca^{2+} amplitude was also diminished in *twk-40(bln336, gf)* mutants (**Figure 3D**).
210 Conversely, in *twk-40(hp834)* loss-of-function mutants, the Ca^{2+} frequency was
211 significantly increased to 5.9±0.5 Hz/300s. Yet, the Ca^{2+} amplitude of *twk-40(hp834)* was
212 unchanged (**Figure 3D**), and the individual Ca^{2+} spike kinetics – including the rise and
213 decay time – were not modified either (**Supplementary Figure S2A-C**), suggesting that
214 *twk-40* contributes to the basal-activity of the DVB neuron. Taken together, our
215 experiments demonstrate that the intrinsic DVB Ca^{2+} oscillation activity was substantially
216 regulated by *twk-40*.
217 To further decipher *twk-40*'s cellular specificity, we firstly measured neuronal Ca^{2+}
218 activity by expressing wild-type TWK-40 cDNA under different exogenous promoters in
219 a *twk-40(bln336, gf)* mutant background. Consistent with our behavioral data, the Ca^{2+}
220 oscillation frequency and amplitude were partially rescued when TWK-40(WT) was
221 expressed in DVB in *twk-40(bln336, gf)* mutants (**Figure 3E-G**). By contrast, neither
222 frequency nor amplitude was restored when TWK-40(WT) was expressed in GABAergic
223 D-motor neurons (**Figure 3G**). In addition, we also expressed TWK-40(WT) in *twk-*
224 *40(hp834)* loss-of-function mutant and found that the increased Ca^{2+} frequency of these

225 mutants could be rescued to wild-type levels when TWK-40(WT) was expressed in DVB
226 neurons (**Figure 3H-J**). Thus, TWK-40(WT) is sufficient to restore the neuronal Ca^{2+}
227 activity of the DVB neurons.

228 Collectively, these results support the notion that *twk-40* regulates neuronal Ca^{2+}
229 oscillations of the DVB neuron.

230 ***twk-40 cell-autonomously regulates DVB Ca^{2+} oscillations***

231 The broad neuronal expression pattern of *twk-40* and a lack of DVB-specific
232 promoters for our rescue experiments did not allow us to directly prove that TWK-40
233 regulates the DMP solely from the DVB neuron (White et al., 1986). To examine whether
234 synaptic input upstream of DVB may play a role, we examined the DVB Ca^{2+} oscillations
235 in an *unc-13(lf)* background. UNC-13 is a conserved and essential presynaptic Ca^{2+}
236 effector that triggers exocytosis and neurotransmitter release. Loss of function of *unc-13*
237 strongly impairs global neurotransmission throughout the nervous system (Brose et al.,
238 1995; Gao and Zhen, 2011; Richmond and Jorgensen, 1999). Interestingly, in the *unc-*
239 *13(lf)* mutant background, we found that Ca^{2+} oscillation defects were retained in *twk-40*
240 mutants, including the decreased frequency and amplitude in *twk-40(bln336, gf)* mutants
241 and increased frequency in *twk-40(hp834, lf)* mutants (**Supplementary Figure S3A-C**).
242 These results demonstrate that presynaptic inputs to DVB don't interfere with the
243 regulation of DVB's Ca^{2+} activities by TWK-40, and that *twk-40* most likely regulates the
244 excitability of DVB neurons in a cell-autonomous manner.

245 To reinforce this notion, we further tested TWK-40's inhibition of DVB by
246 measuring the Ca^{2+} oscillation in transgenic lines that expressed the *twk-40(L159N, gf)*
247 cDNA. When TWK-40(L159N) was expressed in DVB in wild-type animals (driven by

248 P*twk-40* or P*unc-47* promoters), the frequency and amplitude of Ca^{2+} spikes were
249 significantly reduced (**Supplementary Figure S4A**), similar to *twk-40(bln336, gf)*
250 mutants (**Supplementary Figure S4B, C**). By contrast, expression of TWK-40(L159N)
251 in D-motor neurons had no effect. Furthermore, reduced Ca^{2+} oscillations were also
252 observed when TWK-40(L159N) was expressed in a *twk-40(hp834)* loss-of-function
253 mutant background (**Supplementary Figure S4E-F**). These results reveal that ectopic
254 expression of TWK-40(L159N) is sufficient to silence the Ca^{2+} oscillation of DVB
255 neurons. Namely, TWK-40 may execute a dominant inhibition of the intrinsic activity
256 regulation in DVB neuron.

257 ***DVB activity regulates Ca^{2+} dynamics in enteric muscles***

258 The expulsion behavior ultimately relies on the coordinated contraction of a group
259 of muscles, including the anal depressor and sphincter, and two enteric muscles (EM),
260 which wrap around the posterior gut to further pressurize the intestinal contents
261 (McIntire et al., 1993b). EMs are innervated by DVB (**Figure 4Ai**) and AVL neurons
262 (Mclntire et al., 1993, Nature; White et al., 1986), and the contraction of EMs is driven
263 by intracellular Ca^{2+} transients (LeBoeuf and Garcia, 2017). We then ask whether EM
264 Ca^{2+} activity is also regulated in *twk-40* mutants.

265 We thus performed Ca^{2+} imaging of animals expressing the calcium indicator
266 GCaMP6s in the enteric muscles (EM::GCaMP6s, **Figure 4Aii**). As expected, enteric
267 muscles displayed rhythmic Ca^{2+} increases correlated with expulsion. In our experimental
268 conditions, the EM Ca^{2+} spikes exhibited a frequency of 6.4±0.5 Hz/300s (n = 20) in
269 wild-type animals (**Figure 4Aii**). In *twk-40* mutants, the periodicity of EM Ca^{2+} spikes
270 was affected. Specifically, the EM Ca^{2+} spike frequency was significantly reduced in *twk-*

271 *40(bln336, gf)* mutants (3.0±0.2 Hz/300s, n = 20), and increased to 8.6±0.6 Hz/300s (n =
272 20) in *twk-40(hp834, lf)* mutants (**Figure 4B, C**), reminiscent of *twk-40*'s effects for DVB
273 Ca^{2+} frequency. EM Ca^{2+} spike amplitudes, however, were unchanged in *twk-40(bln336,*
274 *gf)* animals (**Figure 4C**), which differs from the reduction observed for DVB Ca^{2+} spike
275 amplitudes (**Figure 3C**). Given that no *twk-40* expression was observed in enteric
276 muscles (**Figure 2B**), we propose that the effects of *twk-40* mutations on the Ca^{2+} activity
277 of enteric muscles are a consequence of the dysregulation of presynaptic DVB neurons.
278 To confirm this idea, we performed additional experiments by expressing wild-type
279 TWK-40 in EM and DVB neurons, respectively. We found that the reduced EM Ca^{2+}
280 frequency in *twk-40(bln336, gf)* mutant was almost fully rescued by expressing TWK-
281 40(WT) in DVB (P*twk-40*::TWK-40(WT) or P*unc-47*::TWK-40(WT)), but not in enteric
282 muscles (P*exp-1*::TWK-40(WT)) or in D-motor neurons (P*unc-25*::TWK-40(WT))
283 (**Figure 4D, E**). Consistently, the increased frequency of EM Ca^{2+} spikes in *twk-*
284 *40(hp834, lf)* mutants was also restored to wild-type by TWK-40(WT) expression in
285 DVB neurons (**Figure 4F, G**). We also ectopically expressed the TWK-40(L159N) gain-
286 of-function in *twk-40(hp834)* animals to inhibit DVB's activity and recorded the EM Ca^{2+}
287 spikes. Consistent with our model, the frequency of EM Ca^{2+} spikes was significantly
288 diminished in this experiment. This inhibition was however not observed in animals
289 expressing TWK-40(L159N) in the enteric muscles or D-motor neurons (**Figure 4H, I**).
290 Collectively, our experiments argue that *twk-40* regulates Ca^{2+} activities of enteric
291 muscles by modulating DVB activity.

292 ***TWK-40 hyperpolarizes the resting membrane potential of DVB neuron***

293 The functional inhibition of DVB neuron by *twk-40* is consistent with an inhibitory
294 function of this potassium channel. To directly investigate the functional effect of *twk-40*,
295 we dissected and recorded GFP-labeled DVB neurons *in vivo* in the whole-cell patch
296 clamp configuration (Methods, **Figure 5A**). In wild-type animals, stable outward K^+
297 currents were recorded at stepwise holding voltages from -60 mV to +80 mV (Xie et al.,
298 2013; Jiang et al., 2021). These currents were significantly diminished in *twk-40(hp834)*
299 loss-of-function mutants (**Figure 5B, C**). Conversely, in *twk-40(bln336)* gain-of-function
300 mutants, outward currents were dramatically increased (**Figure 5B, C**). Thus, these *in-*
301 *situ* neuronal recordings demonstrate that *twk-40* supports a functional K^+ current in DVB
302 neuron.

303 Furthermore, the resting membrane potential (RMP) of DVB was also analyzed.
304 While wild-type DVB neurons had an RMP of -38.9±3.7 mV (n = 6), loss of *twk-40*
305 depolarized the RMP to -22.1±2.9 mV (n = 7). Conversely, in *twk-40(bln336)* mutants,
306 the RMP of DVB neuron was dramatically hyperpolarized to -63.1±5.8 mV (n = 6)
307 (**Figure 5D, E**). Taken together, these results demonstrate that TWK-40 constitutes a K^+
308 channel that stabilizes the RMP of DVB neuron.

309 In summary, we show here that TWK-40 forms a *bona fide* potassium channel that
310 cell-autonomously maintains the RMP of DVB neuron, and that *twk-40* is essential for
311 the regulation of the rhythmic expulsion motor program (**Figure 5F**).

312 **Discussion**

313 Potassium currents mediated by K_{2P} channels are important modulators of neuronal
314 activity in animal nervous systems. We show here that the previously uncharacterized K_{2P}
315 channel TWK-40 provides a prominent leak potassium current in the DVB motor neuron

316 that regulates the rhythmic expulsion behaviour of *C. elegans*. We present genetic
317 evidence that loss of *twk-40* suppresses the *exp* defects of *nlp-40* and *aex-2* mutants.
318 Additional evidence from expression pattern analysis, behavioral rescue experiments, and
319 real-time neuronal and muscular Ca^{2+} imaging, reveal the substantial contribution of
320 TWK-40 to rhythmic expulsion activity. Further proof collected by heterologous
321 expression of TWK-40 (Meng et al., 2022) and *in situ* whole-cell patch clamp recording,
322 demonstrates that *twk-40* constitutes a K_{2P}-like potassium-selective current, and regulates
323 the RMP of DVB neuron. Our results thus identify a K_{2P} channel-dependent cellular
324 mechanism for rhythmic DMP regulation.

325 Circadian rhythms with 24-hour-long cycles like sleeping are well studied and are
326 controlled by the expression fluctuation of clock genes, like *Per1*, *Per2*,and *Bmal1 etc*.
327 (Lowrey and Takahashi, 2004). Ultradian rhythms (or episodic ultradian events) with
328 diverse shorter periods ranging from milliseconds to hours, are ubiquitous and
329 indispensable in many neuromuscular systems, such as heartbeat, respiration and
330 peristalsis (Goh et al., 2019). These ultradian rhythms are generally considered to be
331 generated by motor central pattern generators (CPG) (Marder and Bucher, 2001). The
332 ultradian DMP rhythm in *C. elegans* however is a remarkable exception, as it is initiated
333 by calcium oscillations in intestinal cells (Teramoto and Iwasaki, 2006). The DVB and
334 AVL neurons, acting as a signaling bridge through NLP-40 and GABA pathways,
335 transfer non-neuronal calcium oscillation from the intestine to enteric muscles to execute
336 the expulsion action.

337 Genetic analysis initially highlighted critical ion channel genes for DVB activity,
338 such as *unc-2* and *egl-19* that encode the α1 subunits of P/Q- and L- type voltage-gated

339 Ca^{2+} channel, respectively (Wang and Sieburth, 2013), and *egl-36*, a Shaw-type (Kv3)
340 voltage-dependent potassium channel subunit (Johnstone et al., 1997). However, the *in*
341 *vivo* cellular mechanism of how these channels contribute to the behavior is still
342 unknown. The recent descriptions of synchronized giant action potentials between AVL
343 and DVB, and of unusual compound action potentials in AVL, provide insights into how
344 the rhythmic expulsion behaviour is generated at the cellular level. In particular, the
345 negative potassium spikes in AVL are mediated by a repolarization-activated potassium
346 channel EXP-2 (Jiang et al., 2021). Yet, no ion channel had been associated so far with
347 the rhythmic activity of DVB. Thus, this study identifies TWK-40 as a novel important
348 electrical component for the regulation of the defecation motor program.

349 Among 47 K_{2P} genes in the *C. elegans* genome (Bargmann, 1998), only few have
350 been substantially investigated. Interestingly, nematode K_{2P} channels have been mostly
351 studied using gain-of-function mutations identified in forward genetic screens. For
352 instance, while *twk-18(gf)* mutants cause sluggish, uncoordinated movement (Kunkel et
353 al., 2000), *sup-9(gf)* mutants are hyperactive with a characteristic rubberband phenotype
354 (de la Cruz et al., 2014). Gain-of-function mutants of *unc-58* show significant deficits in
355 locomotion, egg laying, development and aging (Kasap et al., 2018; Salkoff et al., 2005).
356 Except for *twk-18*, we still lack a comprehensive understanding of the electrical
357 properties of these channels *in vitro* and *in vivo*. The recent discovery of a universal
358 activating mutation that promotes the gating of vertebrate and invertebrate K_{2P} channels
359 has opened the way to more comprehensive manipulation of ion channel activity (Ben
360 Soussia et al., 2019). We used this strategy here to engineer a point mutation of TWK-40
361 L159N that achieved a substantial gain-of-function effect. First, we show in a related

362 study that the currents conducted by TWK-40(L159N) channels exhibit ~5 fold increase
363 compared to TWK-40(WT) when heterologously expressed in HEK293 cells (Meng et
364 al., 2022). Second, the resting membrane potential of DVB neurons was drastically
365 hyperpolarized due to the increased outward K^+ current. In this *twk-40(bln336)* gain-of-
366 function mutant, the neuronal Ca^{2+} oscillation frequency and amplitude were reduced,
367 resulting in the significantly diminished expulsion frequency. Thus, our study not only
368 identifies TWK-40 as a regulator of the expulsion rhythm and DVB RMP, but also
369 provides insight into the electrical properties of this K_{2P} channel.

370 We also describe the impact of loss of *twk-40* on the expulsion behavior and DVB
371 activity. In contrast to *gf* mutants, the resting membrane potential of DVB neuron was
372 depolarized in *twk-40(lf)* mutant, and high Ca^{2+} oscillation activity was observed.
373 Consequently, the expulsion number exhibited a moderate but significant increase in *twk-*
374 *40(lf)* mutant. The fact that only few K_{2P} mutants with loss of function phenotypes have
375 been identified in *C. elegans* may be due to functional redundancy between K_{2P} genes.
376 *twk-7* is a notable exception as it exhibits hyperactive locomotion (Gottschling et al.,
377 2017; Luersen et al., 2016). Interestingly, we have found that *twk-40(lf)* mutants also
378 exhibit increased forward and backward body bends, as well as more frequent and
379 prolonged reversals (Meng et al., 2022). A recent genetic study reported that loss of
380 function *twk-40* could reverse the reduced body curvature of *C. elegans NALCN(lf)*
381 mutants (Zhou et al., 2022). Thus, TWK-40 appears to be required for the regulation of
382 multiple motor rhythms.

383 The slight outward-rectification of the *twk-40* dependent K^+ currents in DVB
384 neurons differs from the voltage-independent currents observed in recombinant TWK-40

385 recorded in HEK293 cells (Meng et al., 2022). This could be due to endogenous
386 regulatory subunits expressed in DVB neurons that modify the channel kinetics of TWK-
387 40. Alternatively, TWK-40 could form heteromers with other K_{2P} subunits *in vivo*,
388 resulting in heterodimers with different activation kinetics (Czirjak and Enyedi, 2002).
389 K_{2P} channels can be modulated by a variety of biophysical parameters, such as pH,
390 temperature, and mechanic forces (Enyedi and Czirjak, 2010). Certain K_{2P} channels,
391 including TASK-1/3, TREK-1, and TRESK, are activated by volatile general anesthetics
392 at clinically relevant concentrations (Liu et al., 2004; Patel et al., 1999; Sirois et al.,
393 2000), indicating a major class of drug target from these K_{2P} channels. As a possible
394 ortholog of human TASK-1/3, identification of the critical stimulator of TWK-40 in the
395 future could promote the understanding of how the external environment and internal
396 state affect motor rhythm.

397

398 **Materials and Methods**

399 The complete lists of constructs, transgenic lines and strains generated or acquired for
400 this study are provided in the Supplementary Table 1 and Table 2. All *C. elegans* strains
401 were cultured on standard Nematode Growth Medium (NGM) plates seeded with OP50,
402 and maintained at 22 °C. Unless stated otherwise noted, the wild-type animal refers to the
403 Bristol N2 strain. Only hermaphrodite worms were used for the experiments.

404 ***Constructs and molecular biology***

405 All expression plasmids in this study were constructed by Three-Fragment Multisite
406 Gateway (Invitrogen, Thermo Fisher Scientific, USA) (Magnani et al., 2006). Three-
407 Fragment Multisite gateway system consists of three entry clones. Three entry clones

408 comprising three PCR products (promoter, target gene, sl2-GFP or unc-54 3'UTR, in
409 name of slot 1, slot 2 and slot 3, respectively) were recombined into the pDEST-R4-R3 or
410 pDEST-R4-R3-unc-54 3'UTR destination vectors by using standard LR recombination
411 reactions to generate the expression clones.

412 All promoters used in this study were generated by PCR against a mixed-stage N2
413 *C. elegans* genomic DNA. Promoters include the 1.4 kb P*twk-40*, 1.2 kb P*unc-47*, 1.8 kb
414 P*unc-25*, 2.4 kb P*exp-1* and 1.4 kb P*ges-1* genomic sequence upstream of the respective
415 ATG start codon and were used to substitute for the *rab-3* fragment in standard BP
416 reaction-generated entry clone A with the In-Fusion method, using ClonExpress® II One
417 Step Cloning Kit (Vazyme, China). The used 1.8 kb short promoter of P*unc-25* is only
418 expressed in D-motor neurons (unpublished).

419 To generate the entry clones slot 2 and slot 3, we used standard BP recombination
420 reactions. An entry clone B contributing sequences of slot 2 in the expression plasmid
421 contains sequence of a target gene, i.e., *twk-40*, GFP, or RFP. The "B" entry clones were
422 constructed by the use of *pDONR™ 221* donor vector (Invitrogen) through BP reactions.
423 All the DNA fragments used to construct entry clone B involved in this project were
424 amplified by PCR with the primers containing attB1 and attB2 recombination sites.

425 An entry clone "C" contributing sequences of slot 3 in the expression plasmids
426 contains a sequence of *unc-54* 3' UTR, *sl2d*-GFP or *sl2d*-wCherry. The "C" entry clones
427 were constructed by use of *pDONR-P2R-P3* donor vector through standard BP reactions.
428 The corresponding PCR products with attB2R and attB3 sites were amplified by PCR.

429 For calcium imaging, constructs with genetic calcium sensor GCaMP6.0s were
430 used for neuronal activity measurement. The GCaMP6.0s sequence (Chen et al., 2013)

431 was codon-optimized for expression in *C. elegans*. The synthesized gene also contains
432 three *C. elegans* introns and contain restriction enzyme sites to facilitate subsequent
433 cloning. In all constructs, GCaMP6.0s was fused in frame with a *C. elegans* codon-
434 optimized wCherry at the C-terminus to allow ratio metric measurement via simultaneous
435 imaging of GFP and RFP.

436 ***Genetic mutants and transgenetic arrays***

437 Loss-of-function allele *hp834* was generated by targeted CRISPR/Cas9 genome editing
438 with a 7 bp deletion of the sequence (GTTCGAG, base 127-133) was introduced in the
439 2nd exon of T28A8.1a. *twk-40(bln336)* was generated by CRISPR/Cas9 technology by
440 mutating 1047-1048 base of T28A8.1a from CT to AA. Other genetic mutants used for
441 constructing transgenic lines and compound mutants were obtained from the
442 *Caenorhabditis Genetics Center* (*CGC*). Transgenic animals that carry non-integrated,
443 extra-chromosomal arrays (*gaaEx*) were generated by co-injecting an injection marker
444 with one to multiple DNA construct at 5-30 ng/µl. All animals were backcrossed at least
445 four times against N2 prior to analyses.

446 ***Behavioral assay for the defecation motor program***

447 A single 12-18 hr post-L4 stage adult hermaphrodite, maintained on standard culture
448 conditions, was transferred to a fresh NMG plate and let to settle down for at least five
449 minutes. Count the number of pBoc and Exp steps in 10 minutes. Each genotype assays
450 were repeated at least in 10 worms. "Exp per cycle" for each worm was calculated as the
451 ratio of Exp over pBoc.

452 ***Fluorescence Microscopy***

453 Images of fluorescently tagged proteins were captured in live L4 worms. L4 stage
454 transgenic animals expressing fluorescence markers were picked a day before imaging.
455 Worms were immobilized by 2.5 mM levamisole (Sigma-Aldrich, USA) in M9 buffer.
456 Fluorescence signals were captured from live worms using a Plan-Apochromatic 60X
457 objective on a confocal microscope (FV3000, Olympus, Japan) in the same conditions.

458 ***Calcium imaging***

459 The genetic calcium indicator GCaMP6.0s was used for neuronal calcium imaging in this
460 study. To simplify the experiment, animals are glued down on the cover glass as
461 described for electrophysiological recording but leave the tail free (Gao et al., 2015). The
462 defecation motor program did not show significant difference between immobilized intact
463 animals and free moving animals. GFP fluorescence from GCaMP in DVB and intestine
464 muscles from immobilized animals was collected with a 60X water objective (Nikon,
465 Japan) and recorded by a sCMOS digital camera (Hamamatsu ORCA-Flash 4.0V2,
466 Japan) at 100 ms per frame. Custom MATLAB scripts were used to extract the pixel
467 intensity for each frame. $\Delta F/F$ was used to calculate the relative fluorescence intensity
468 change, and analyzed by MicroManager and Image J.

469 ***In-situ electrophysiology***

470 Dissection and recording were carried out using protocols and solutions described in the
471 previous studies (Gao and Zhen, 2011; Richmond and Jorgensen, 1999; Mellem et al.,
472 2008). Briefly, 1- or 2-day-old hermaphrodite adults were glued (Histoacryl Blue, Braun,
473 Germany) to a sylgard-coated cover glass covered with bath solution (Sylgard 184,
474 Dowcorning, USA) under stereoscopic microscope M50 (Leica, Germany). After clearing
475 the viscera by suction through a glass pipette, the cuticle flap was turned and gently glued

476 down using WORMGLU (GluStitch Inc., Canada) to expose the neuromuscular system.
477 The integrity of the ventral nerve cord were visually examined via DIC microscopy
478 (Eclipse FN1, Nikon, Japan), and DVB neuron were patched using 15-20 MΩ-resistant
479 borosilicate pipettes (1B100F-4, World Precision Instruments, USA). Pipettes were
480 pulled by micropipette puller P-1000 (Sutter, USA), and fire-polished by microforge MF-
481 830 (Narishige, Japan). Membrane potential, I-V curve and action potentials were
482 recorded in the whole-cell configuration by EPC9 amplifier (HEKA, Germany), using the
483 pulse and processed with Igor Pro (WaveMetrics, USA) and Clampfit 10 software (Axon
484 Instruments, Molecular Devices, USA). Membrane potential was recorded at 0 pA, action
485 potentials was recorded from 0 pA to 100 pA, I-V curve was recorded at holding
486 potential from –60 mV to 80mV at 20 mV increment. Data were digitized at 10–20 kHz
487 and filtered at 2.6 kHz. The pipette solution contains (in mM): K-gluconate 115; KCl 25;
488 $CaCl_2$ 0.1; $MgCl_2$ 5; BAPTA 1; HEPES 10; Na_2ATP 5; Na_2GTP 0.5; cAMP 0.5; cGMP
489 0.5, pH7.2 with KOH, ~320 mOsm. cAMP and cGMP were included to maintain the
490 activity and longevity of the preparation. The bath solution consists of (in mM): NaCl
491 150; KCl 5; $CaCl_2$ 5; $MgCl_2$ 1; glucose 10; sucrose 5; HEPES 15, pH7.3 with NaOH,
492 ~330 mOsm. Chemicals were obtained from Sigma unless stated otherwise. Experiments
493 were performed at room temperatures (20-22 °C).

494 ***Statistical analysis***

495 The two-tailed Student's *t*-test were used to compare data sets. $P < 0.05$ was considered
496 to be statistically significant; *, ** and *** denote $P < 0.05$, $P < 0.01$, $P < 0.001$,
497 respectively. Graphing and subsequent analysis were performed using Igor Pro
498 (WaveMetrics), Clampfit (Molecular Devices), Image J (National Institutes of Health),

499 Python, Matlab (MathWorks, USA), GraphPad Prism 8 (GraphPad Software Inc., USA)
500 and Excel (Microsoft, USA). For behavior analysis, calcium imaging, electrophysiology
501 and fluorescence imaging, each recording trace was obtained from a different animal.
502 Unless specified otherwise, data were presented as the mean ± SEM.

503 **Author Contributions**

504 S.G. conceived experiments and wrote the manuscript. Z.Y., Y.Z., B.Y., and Y.X.
505 performed experiments and analyzed data. L.C., Y.L., J. C. J.M., W.H., S.E.M, T.B., and
506 C.Z. contributed to the experiments. T.B. and M.Z. provided reagents, discussed the
507 experiments and edited the text.

508 **Acknowledgements**

509 We thank Gao lab members for comments and discussion. This research was supported
510 by the National Natural Science Foundation of China (31871069), the Major International
511 (Regional) Joint Research Project (32020103007), the Overseas High-level Talents
512 Introduction Program, and the European Research Council (TB, ERC Starting Grant,
513 Kelegans). We thank *Caenorhabditis Genetics Center*, which is funded by the NIH
514 Office of Research Infrastructure Programs (P40 OD010440), for strains.

515 **Declaration of Interests**

516 The authors declare no conflict of interest.

517 **References**

518 Bargmann, C.I. (1998). Neurobiology of the Caenorhabditis elegans genome. Science
519 *282*, 2028-2033.

520 Beg, A.A., and Jorgensen, E.M. (2003). EXP-1 is an excitatory GABA-gated cation
521 channel. Nat Neurosci *6*, 1145-1152.

522 Ben Soussia, I., El Mouridi, S., Kang, D., Leclercq-Blondel, A., Khoubza, L., Tardy, P.,
523 Zariohi, N., Gendrel, M., Lesage, F., Kim, E.J.*, et al.* (2019). Mutation of a single residue
524 promotes gating of vertebrate and invertebrate two-pore domain potassium channels. Nat
525 Commun *10*, 787.

526 Branicky, R., and Hekimi, S. (2006). What keeps C. elegans regular: the genetics of
527 defecation. Trends Genet *22*, 571-579.

528 Brose, N., Hofmann, K., Hata, Y., and Sudhof, T.C. (1995). Mammalian homologues of
529 Caenorhabditis elegans unc-13 gene define novel family of C2-domain proteins. J Biol
530 Chem *270*, 25273-25280.

531 Buckingham, S.D., Kidd, J.F., Law, R.J., Franks, C.J., and Sattelle, D.B. (2005).
532 Structure and function of two-pore-domain K^+ channels: contributions from genetic
533 model organisms. Trends Pharmacol Sci *26*, 361-367.

534 Chen, T.W., Wardill, T.J., Sun, Y., Pulver, S.R., Renninger, S.L., Baohan, A., Schreiter,
535 E.R., Kerr, R.A., Orger, M.B., Jayaraman, V.*, et al.* (2013). Ultrasensitive fluorescent
536 proteins for imaging neuronal activity. Nature *499*, 295-300.

537 Choi, U., Wang, H., Hu, M., Kim, S., and Sieburth, D. (2021). Presynaptic coupling by
538 electrical synapses coordinates a rhythmic behavior by synchronizing the activities of a
539 neuron pair. Proc Natl Acad Sci U S A *118*.

540 Cook, S.J., Jarrell, T.A., Brittin, C.A., Wang, Y., Bloniarz, A.E., Yakovlev, M.A.,
541 Nguyen, K.C.Q., Tang, L.T., Bayer, E.A., Duerr, J.S.*, et al.* (2019). Whole-animal
542 connectomes of both Caenorhabditis elegans sexes. Nature *571*, 63-71.

543 Czirjak, G., and Enyedi, P. (2002). Formation of functional heterodimers between the
544 TASK-1 and TASK-3 two-pore domain potassium channel subunits. J Biol Chem *277*,
545 5426-5432.

546 Dal Santo, P., Logan, M.A., Chisholm, A.D., and Jorgensen, E.M. (1999). The inositol
547 trisphosphate receptor regulates a 50-second behavioral rhythm in C. elegans. Cell *98*,
548 757-767.

549 de la Cruz, I.P., Ma, L., and Horvitz, H.R. (2014). The Caenorhabditis elegans
550 iodotyrosine deiodinase ortholog SUP-18 functions through a conserved channel SC-box
551 to regulate the muscle two-pore domain potassium channel SUP-9. PLoS Genet *10*,
552 e1004175.

553 Enyedi, P., and Czirjak, G. (2010). Molecular background of leak K^+ currents: two-pore
554 domain potassium channels. Physiol Rev *90*, 559-605.

555 Gao, S., Xie, L., Kawano, T., Po, M.D., Guan, S., Zhen, M., Pirri, J.K., and Alkema, M.J.
556 (2015). The NCA sodium leak channel is required for persistent motor circuit activity that
557 sustains locomotion. Nat Commun *6*, 6323.

558 Gao, S., and Zhen, M. (2011). Action potentials drive body wall muscle contractions in
559 Caenorhabditis elegans. Proc Natl Acad Sci U S A *108*, 2557-2562.

560 Goh, G.H., Maloney, S.K., Mark, P.J., and Blache, D. (2019). Episodic Ultradian Events-
561 Ultradian Rhythms. Biology (Basel) *8*.

562 Goldstein, S.A., Bayliss, D.A., Kim, D., Lesage, F., Plant, L.D., and Rajan, S. (2005).
563 International Union of Pharmacology. LV. Nomenclature and molecular relationships of
564 two-P potassium channels. Pharmacol Rev *57*, 527-540.

565 Gottschling, D.C., Doring, F., and Luersen, K. (2017). Locomotion Behavior Is Affected
566 by the GalphaS Pathway and the Two-Pore-Domain K^+ Channel TWK-7 Interacting in
567 GABAergic Motor Neurons in Caenorhabditis elegans. Genetics *206*, 283-297.

568 Graham, J.M., Jr., Zadeh, N., Kelley, M., Tan, E.S., Liew, W., Tan, V., Deardorff, M.A.,
569 Wilson, G.N., Sagi-Dain, L., and Shalev, S.A. (2016). KCNK9 imprinting syndrome-
570 further delineation of a possible treatable disorder. Am J Med Genet A *170*, 2632-2637.

571 Jiang, J., Su, Y., Zhang, R., Li, H., Tao, L.,and Liu, Q. (2021). C. elegans enteric motor
572 neurons fire synchronized action potentials underlying the defecation motor program.
573 bioRxiv doi: https://doi.org/10.1101/2021.08.25.457687.

574 Johnstone, D.B., Wei, A., Butler, A., Salkoff, L., and Thomas, J.H. (1997). Behavioral
575 defects in C. elegans egl-36 mutants result from potassium channels shifted in voltage-
576 dependence of activation. Neuron *19*, 151-164.

577 Kasap, M., Weeks, K., Aamodt, E.J., and Dwye, D.S. (2018). Gain-of-function mutations
578 in a two-pore domain K^+ channel(unc-58) cause developmental, motor and feeding
579 defects in C. elegans modified by temperature and a channel inhibitor,loratadine. Curr
580 Neurobiol *9*, 84-91.

581 Kunkel, M.T., Johnstone, D.B., Thomas, J.H., and Salkoff, L. (2000). Mutants of a
582 temperature-sensitive two-P domain potassium channel. J Neurosci *20*, 7517-7524.

583 Lalevee, N., Monier, B., Senatore, S., Perrin, L., and Semeriva, M. (2006). Control of
584 cardiac rhythm by ORK1, a Drosophila two-pore domain potassium channel. Curr Biol
585 *16*, 1502-1508.

586 LeBoeuf, B., and Garcia, L.R. (2017). Caenorhabditis elegans Male Copulation Circuitry
587 Incorporates Sex-Shared Defecation Components To Promote Intromission and Sperm
588 Transfer. G3 (Bethesda) *7*, 647-662.

589 Lee, J., Song, H.O., Jee, C., Vanoaica, L., and Ahnn, J. (2005). Calcineurin regulates
590 enteric muscle contraction through EXP-1, excitatory GABA-gated channel, in C.
591 elegans. J Mol Biol *352*, 313-318.

592 Lesage, F., and Lazdunski, M. (2000). Molecular and functional properties of two-pore-
593 domain potassium channels. Am J Physiol Renal Physiol *279*, F793-801.

594 Liu, C., Au, J.D., Zou, H.L., Cotten, J.F., and Yost, C.S. (2004). Potent activation of the
595 human tandem pore domain K channel TRESK with clinical concentrations of volatile
596 anesthetics. Anesth Analg *99*, 1715-1722.

597 Liu, D.W., and Thomas, J.H. (1994). Regulation of a periodic motor program in C.
598 elegans. J Neurosci *14*, 1953-1962.

599 Lowrey, P.L., and Takahashi, J.S. (2004). Mammalian circadian biology: elucidating
600 genome-wide levels of temporal organization. Annu Rev Genomics Hum Genet *5*, 407-
601 441.

602 Luersen, K., Gottschling, D.C., and Doring, F. (2016). Complex Locomotion Behavior
603 Changes Are Induced in Caenorhabditis elegans by the Lack of the Regulatory Leak K^+
604 Channel TWK-7. Genetics *204*, 683-701.

605 Magnani, E., Bartling, L., and Hake, S. (2006). From Gateway to MultiSite Gateway in
606 one recombination event. BMC Mol Biol *7*, 46.

607 Mahoney, T.R., Luo, S., Round, E.K., Brauner, M., Gottschalk, A., Thomas, J.H., and
608 Nonet, M.L. (2008). Intestinal signaling to GABAergic neurons regulates a rhythmic
609 behavior in Caenorhabditis elegans. Proc Natl Acad Sci U S A *105*, 16350-16355.

610 Marder, E., and Bucher, D. (2001). Central pattern generators and the control of rhythmic
611 movements. Curr Biol *11*, R986-996.

612 Marder, E., and Calabrese, R.L. (1996). Principles of rhythmic motor pattern generation.
613 Physiol Rev *76*, 687-717.

614 McIntire, S.L., Jorgensen, E., and Horvitz, H.R. (1993a). Genes required for GABA
615 function in Caenorhabditis elegans. Nature *364*, 334-337.

616 McIntire, S.L., Jorgensen, E., Kaplan, J., and Horvitz, H.R. (1993b). The GABAergic
617 nervous system of Caenorhabditis elegans. Nature *364*, 337-341.

618 Meng, J., Su, Y., Zhang, R., Li, H., Gao, S.,and Zhen, M. (2022). C. elegans enteric
619 motor neurons fire synchronized action potentials underlying the defecation motor
620 program. bioRxiv doi: https://doi.org/10.1101/2021.08.25.457687.

621 Nehrke, K., Denton, J., and Mowrey, W. (2008). Intestinal Ca^{2+} wave dynamics in freely
622 moving C. elegans coordinate execution of a rhythmic motor program. Am J Physiol Cell
623 Physiol *294*, C333-344.

624 Patel, A.J., Honore, E., Lesage, F., Fink, M., Romey, G., and Lazdunski, M. (1999).
625 Inhalational anesthetics activate two-pore-domain background K^+ channels. Nat Neurosci
626 *2*, 422-426.

627 Richmond, J.E., and Jorgensen, E.M. (1999). One GABA and two acetylcholine receptors
628 function at the C. elegans neuromuscular junction. Nat Neurosci *2*, 791-797.

629 Salkoff, L., Butler, A., Fawcett, G., Kunkel, M., McArdle, C., Paz-y-Mino, G., Nonet,
630 M., Walton, N., Wang, Z.W., Yuan, A.*, et al.* (2001). Evolution tunes the excitability of
631 individual neurons. Neuroscience *103*, 853-859.

632 Salkoff, L., Wei, A.D., Baban, B., Butler, A., Fawcett, G., Ferreira, G., and Santi, C.M.
633 (2005). Potassium channels in C. elegans. WormBook, 1-15.

634 Sirois, J.E., Lei, Q., Talley, E.M., Lynch, C., 3rd, and Bayliss, D.A. (2000). The TASK-1
635 two-pore domain K^+ channel is a molecular substrate for neuronal effects of inhalation
636 anesthetics. J Neurosci *20*, 6347-6354.

637 Teramoto, T., and Iwasaki, K. (2006). Intestinal calcium waves coordinate a behavioral
638 motor program in C. elegans. Cell Calcium *40*, 319-327.

639 Thomas, J.H. (1990). Genetic analysis of defecation in Caenorhabditis elegans. Genetics
640 *124*, 855-872.

641 Wang, H., Girskis, K., Janssen, T., Chan, J.P., Dasgupta, K., Knowles, J.A., Schoofs, L.,
642 and Sieburth, D. (2013). Neuropeptide secreted from a pacemaker activates neurons to
643 control a rhythmic behavior. Curr Biol *23*, 746-754.

644 Wang, H., and Sieburth, D. (2013). PKA controls calcium influx into motor neurons
645 during a rhythmic behavior. PLoS genetics *9*, e1003831.

646 Wang, Z.W., Kunkel, M.T., Wei, A., Butler, A., and Salkoff, L. (1999). Genomic
647 organization of nematode 4TM K^+ channels. Ann N Y Acad Sci *868*, 286-303.

648 White, J.G., Southgate, E., Thomson, J.N., and Brenner, S. (1986). The structure of the
649 nervous system of the nematode Caenorhabditis elegans. Philos Trans R Soc Lond B Biol
650 Sci *314*, 1-340.

651 Witvliet, D., Mulcahy, B., Mitchell, J.K., Meirovitch, Y., Berger, D.R., Wu, Y., Liu, Y.,
652 Koh, W.X., Parvathala, R., Holmyard, D.*, et al.* (2021). Connectomes across
653 development reveal principles of brain maturation. Nature *596*, 257-261.

654 Zhou, C., Zhou, Q., He, X., He, Y., Wang, X., Zhu, X., Zhang, Y., Ma, L. (2022).
655 Differential modulation of C. elegans motor behavior by NALCN and two-pore domain
656 potassium channels. PLOS Genetics *18*, e1010126.

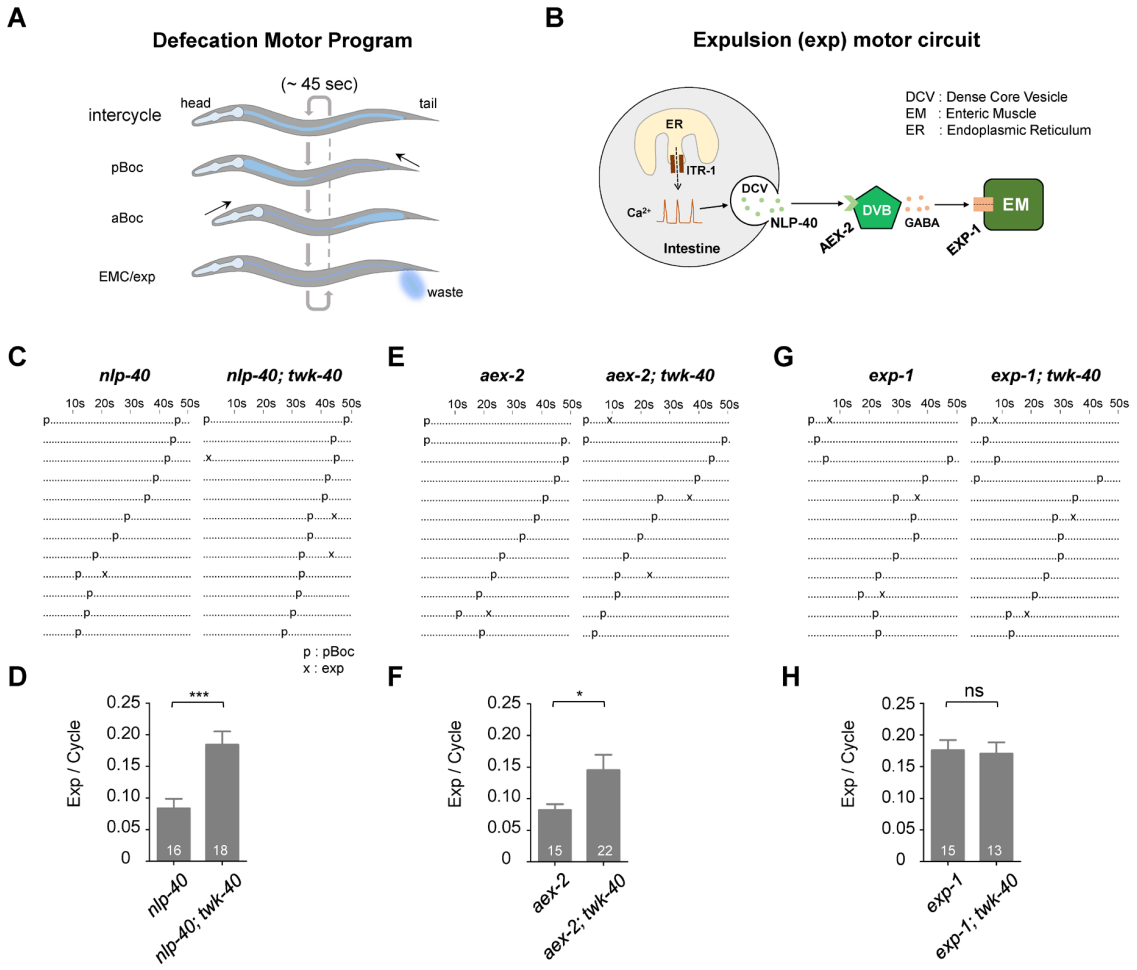

Figure 1. Loss of function of twk-40 suppresses expulsion defects in nlp-40 and aex-2 mutants

(**A**) Schematic representation of the defecation motor program (DMP), which consists of three distinct sets of muscle contractions: the posterior body muscle contraction (pBoc), the anterior body muscle contraction (aBoc), and the expulsion muscle contraction (exp or EMC). The regular defecation cycle period is approximately 45 sec. (**B**) Schematic representation of the expulsion motor circuit, including the intestine, DVB neuron and enteric muscles (EM). ER, endoplasmic reticulum; ITR-1, inositol 1,4,5-trisphosphate receptor; DCV: dense core vesicle. (**C, E, G**) Ethograms of defecation behavior in *nlp-40* and *nlp-40; twk-40* double mutants, *aex-2* and *aex-2; twk-40* double mutants, and *exp-1*

668 and *exp-1; twk-40* double mutants, respectively. Each dot and character represent 1 s.
669 Letters ‘p’ and ‘x’ represent pBoc and exp, respectively. (**D, F, H**) Quantifications of the
670 expulsion frequency per defecation cycle. The expulsion deficiency was partially
671 recovered by loss of *twk-40* in *nlp-40* and *aex-2* mutants, but not in *exp-1* mutants. All
672 data are expressed as means ± SEM. Student’s *t*-test was used. Statistical significance is
673 indicated as follows: ns, not significant, $*P < 0.05$, $***P < 0.001$ in comparison with that
674 as denoted.

675

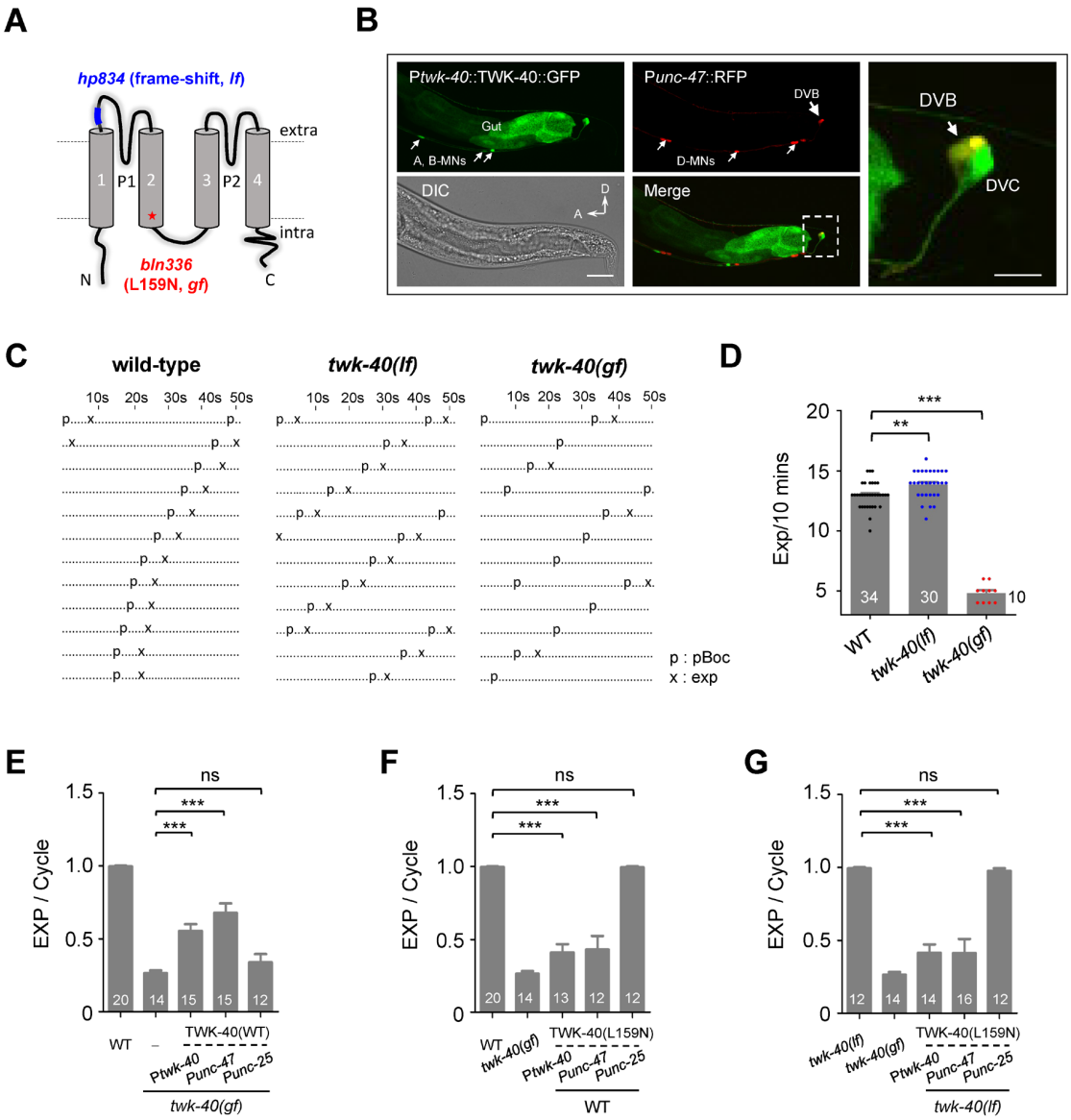

676

677 ***Figure 2. twk-40 regulates expulsion rhythm from DVB neuron***

678 (**A**) Diagram of the TWK-40 K^+ channel and the mutation loci. P1 and P2, pore domains;

679 1-4 transmembrane domains; *fs*, predicted frameshift mutation; *gf*, gain-of-function

680 mutation. (**B**) *twk-40* is expressed in DVB based on co-localization of P*twk-40*::TWK-

681 40::sl2dGFP and P*unc-47*::RFP. GFP was observed in the ventral excitatory motor

682 neurons, a few head and tail neurons, and the intestine. Scale bar, 20 µm. *Right*, zoomed

683 view of *twk-40* expression in DVB and DVC. Scale bar, 5 μm. (**C**) Ethograms of
684 defecation behavior in wild type, *twk-40(bln336, gf)* and *twk-40(hp834, lf)* animals. Each
685 dot and character represent 1 s. Letters 'p' and 'x' represent pBoc and exp, respectively.
686 (**D**) Quantifications of the expulsion frequency per defecation cycle. Compared to wild-
687 type animals, the expulsion deficiency was significantly reduced in *twk-40(bln336, gf)*,
688 but not in *twk-40(hp834, lf)*. (**E**) Neuronal expression of wild-type TWK-40 (TWK-
689 40(WT)) in DVB neurons rescues the expulsion deficiency of *twk-40(bln336, gf)*
690 mutants. (**F, G**) Neuronal expression of gain-of-function TWK-40(L159N) in DVB in
691 wild type (F) or *twk-40(hp834)* (G) recapitulates the expulsion deficiency of *twk-40(gf)*
692 mutant. The number of tested animals is indicated for each strain. All data are expressed
693 as means ± SEM. Student's *t*-test was used, in which: ns, not significant, $^{**}P < 0.01$,
694 $^{***}P < 0.001$ relative to wild type or as indicated.

695

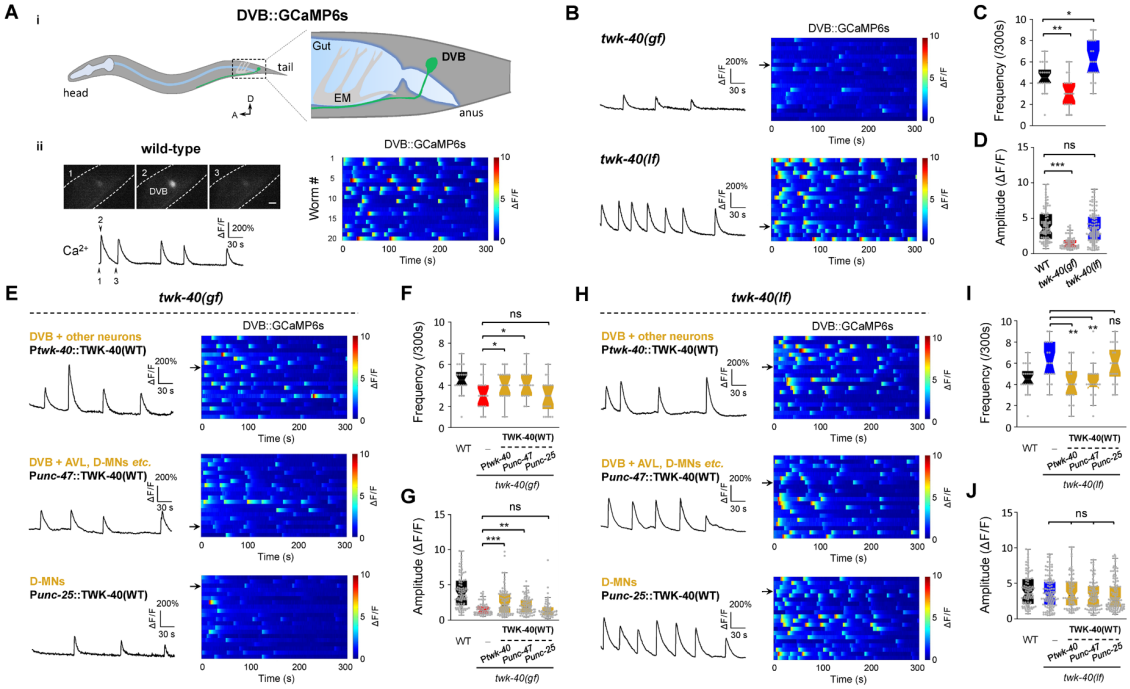

696

697 ***Figure 3. twk-40 inhibits DVB Ca^{2+} oscillation***

698 (**A**) i. Schematic representation of *C. elegans* DVB neuron and enteric muscle (EM) in a

699 lateral view. The genetically-encoded Ca^{2+} indicator GCaMP6.0s was expressed in DVB

700 to measure its neuronal activity. ii. Representative spontaneous Ca^{2+} oscillation imaged

701 by GCaMP in DVB neuron *in-vivo*. *Upper*, from left to right, Ca^{2+} signal of DVB in (1)

702 the quiescent state, (2) at peak Ca^{2+} signal and (3) upon return to the basal state. Scale

703 bar, 5 µm. *Bottom*, representative recording of Ca^{2+} oscillations in DVB over time. Arrow

704 heads indicate the corresponding time points in upper panels. Color map of the Ca^{2+}

705 oscillations in wild-type animals. (**B**) Representative Ca^{2+} activity (*left*) and color maps

706 (*right*) of DVB neurons in *twk-40(bln336, gf)* and *twk-40(hp834, lf)* mutants,

707 respectively. (**C, D**) Significant reduction of Ca^{2+} transient frequency and amplitude in

708 *twk-40(bln336, gf)* mutant, n=20. Reduction of frequency but not amplitude in *twk-*

709 *40(hp834, lf)* mutants. (**E**) Representative DVB Ca^{2+} traces (*left*) and color maps (*right*)

710 for tissue-specific expression of TWK-40(WT) in *twk-40(bln336, gf)* mutants. *Upper*,
711 endogenous promoter P*twk-40*; *middle*, P*unc-47* promoter including DVB expression;
712 *bottom*, P*unc-25* promoter lacking DVB expression. (**F, G**) Quantification of the
713 frequency and amplitude of Ca^{2+} transients, n=20. (**H**) Representative DVB Ca^{2+} traces
714 (*left*) and color maps (*right*) for tissue-specific expression of TWK-40(WT) in *twk-*
715 *40(hp834, lf)* mutant. (**F, G**) Quantification of the frequency and amplitude of Ca^{2+}
716 transients, n=20. All data are expressed as means ± SEM. Student's *t*-test was used, in
717 which: ns, not significant, *$P < 0.05$, **$P < 0.01$, ***$P < 0.001$ in comparison with that
718 as denoted.

719

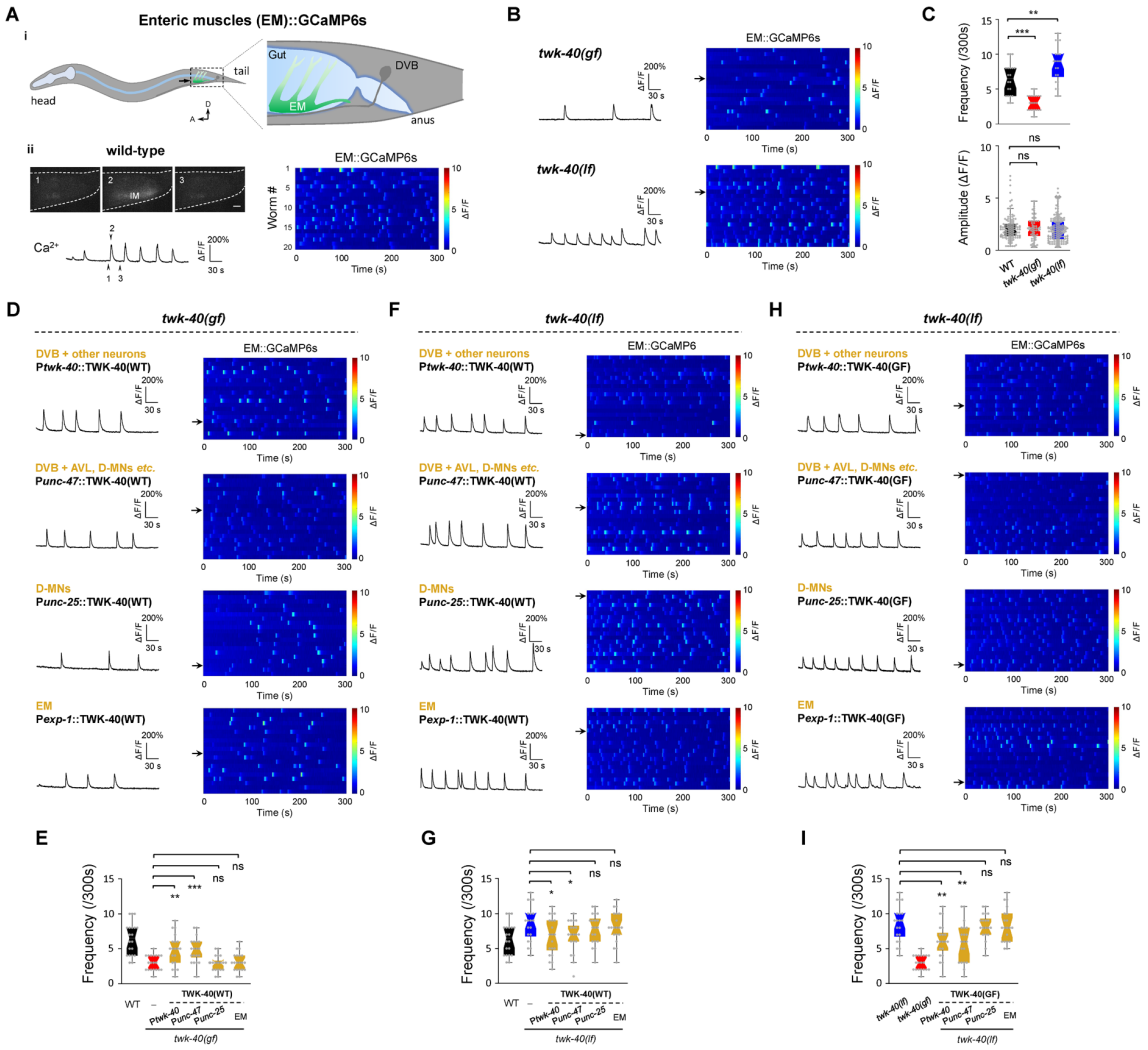

Figure 4. Disruption of Ca^{2+} dynamics in enteric muscles of twk-40 mutants

(**A**) *i*. Schematic representation of *C. elegans* DVB neuron and enteric muscle (EM) in a lateral view. The genetically-encoded Ca^{2+} indicator GCaMP6.0s was expressed in EM. *ii*. Representative Ca^{2+} oscillation imaged by GCaMP in EM *in-vivo*. *Upper*, from left to right, Ca^{2+} signal of EM in (1) the quiescent state, (2) at peak Ca^{2+} signal and (3) upon return to the basal state. Scale bar, 5 µm. *Bottom*, representative recording of Ca^{2+} oscillations in EM over time. Arrow heads indicate the corresponding time points in upper panels. Color map of the rhythmic EM Ca^{2+} activities in wild-type animals. (**B**)

729 Representative Ca^{2+} activity (*left*) and color maps (*right*) of enteric muscles in *twk-*
730 *40(bln336, gf)* and *twk-40(hp834, lf)* mutants, respectively. (**C**) Quantification of EM
731 Ca^{2+} transients frequency and amplitude , n=20. Ca^{2+} transient frequency was
732 significantly reduced in *twk-40(bln336, gf)* mutant, but was increased in *twk-40(hp834, lf)*
733 mutant. EM Ca^{2+} amplitude was not altered in either mutants. (**D, F**) Representative EM
734 Ca^{2+} traces (*left*) and color maps (*right*) in *twk-40(bln336, gf)* (E) and *twk-40(hp834, lf)*
735 (G) for tissue-specific expression of TWK-40(WT). 1, endogenous promoter P*twk-40*; 2,
736 P*unc-47* promoter including DVB expression; 3, P*unc-25* promoter lacking DVB
737 expression; 4, P*exp-1* promoter for enteric muscle expression. (**E, G**) Rescue of EM Ca^{2+}
738 transient frequency by expression of TWK-40(WT) in DVB, but not enteric muscles or
739 other neurons, n=20. (**H**) Representative EM Ca^{2+} traces (*left*) and color maps (*right*) in
740 *twk-40(hp834, lf)* following tissue-specific expression of TWK-40(L159N). (**I**) Reduction
741 of EM Ca^{2+} transient frequency following TWK-40(L159N) expression in DVB, but not
742 enteric muscles or other neurons, n=20. All data are expressed as means ± SEM.
743 Student's *t*-test was used, in which: ns, not significant, $*P < 0.05$, $**P < 0.01$, $***P <$
744 0.001 in comparison with that as denoted.

745

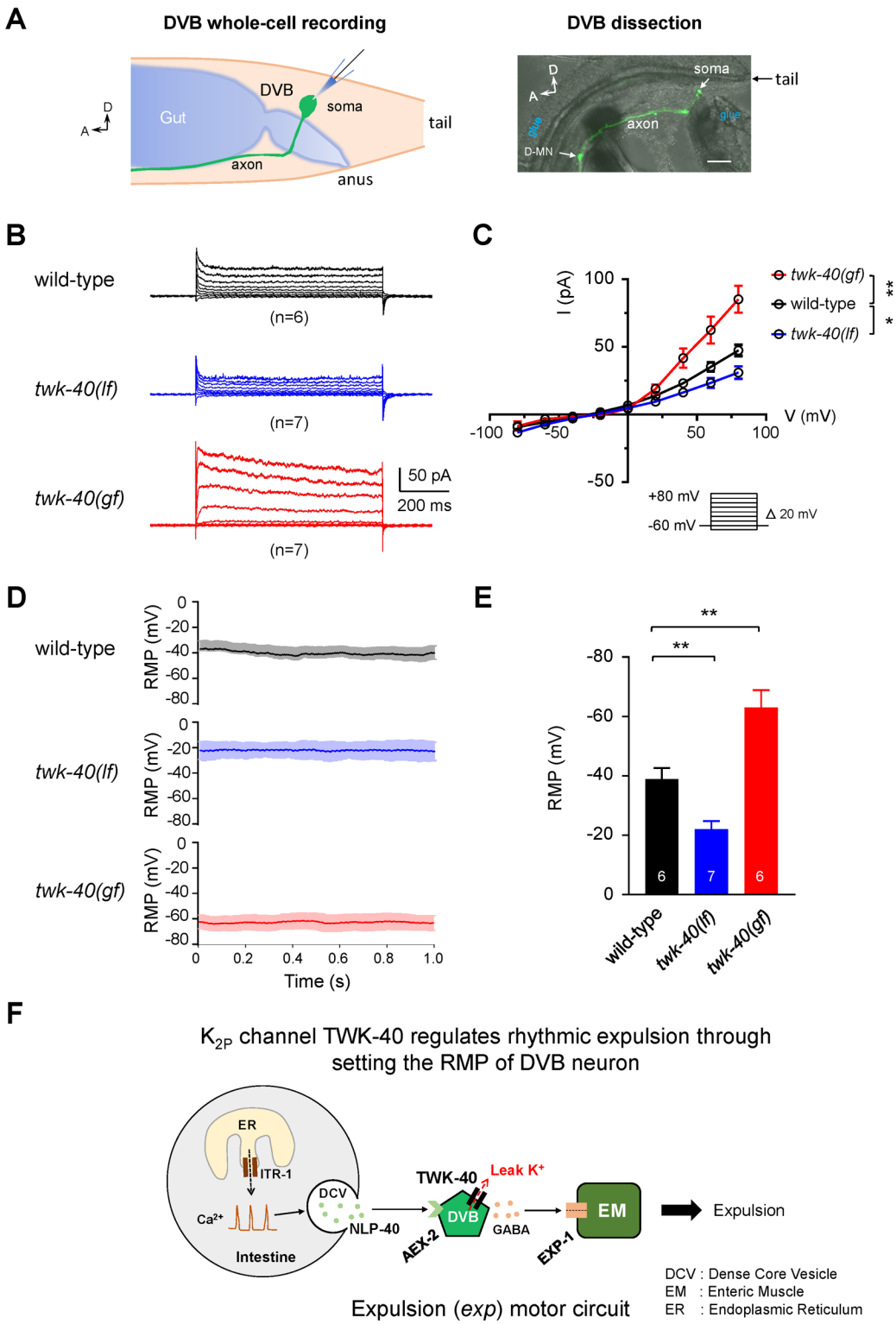

746

747 ***Figure 5. TWK-40 hyperpolarizes the DVB neuron.***

748 (**A**) *Left*, schematic representation of *C. elegans* DVB neuron for whole-cell patch clamp
749 recording. *Right*, GFP-labeled DVB soma and axon. (**B**) Representative outward K^+
750 currents recorded from DVB neurons in different genotypes. (**C**) Quantification of the
751 current-voltage curves from different genotypes reveals that the outward currents were
752 reduced in *twk-40(hp834, lf)* mutant, but increased in *twk-40(bln336, gf)* mutant. (**D, E**)
753 Representative traces and quantification of the resting membrane potential (RMP)
754 recorded from DVB in different genotypes. (**F**) The working Model: K_{2P} channel TWK-
755 40 regulates the rhythmic expulsion behavior by setting the resting membrane potential of
756 DVB neuron. Student's *t*-test was used to test the significant difference of average
757 currents at +80 mV, in which: ns, not significant, $*P < 0.05$, $**P < 0.01$ in comparison
758 with that as denoted.